Article

Photocatalytic Transformations of the Resveratrol Derivative in Microflow Reactor

Milena Mlakić [1], Anabela Ljubić [2], Anita Šalić [3,*], Bruno Zelić [4,5], Ottó Horváth [6], Valentina Milašinović [7], Martin Gojun [4], Krešimir Molčanov [7] and Irena Škorić [1,*]

1 Department of Organic Chemistry, Faculty of Chemical Engineering and Technology, University of Zagreb, Marulićev Trg 19, HR-10 000 Zagreb, Croatia
2 Pliva R&D, Teva Pharmaceutical Industries Ltd., Prilaz baruna Filipovića 29, HR-10 000 Zagreb, Croatia
3 Department of Thermodynamics, Mechanical Engineering and Energy, Faculty of Chemical Engineering and Technology, University of Zagreb, Marulićev trg 19, HR-10 000 Zagreb, Croatia
4 Department of Reaction Engineering and Catalysis, Faculty of Chemical Engineering and Technology, University of Zagreb, Marulićev Trg 19, HR-10 000 Zagreb, Croatia
5 Department of Packaging, Recycling and Environmental Protection, University North, Trg dr. Žarka Dolinara 1, HR-48 000 Koprivnica, Croatia
6 Environmental and Inorganic Photochemistry Research Group, Center for Natural Sciences, Faculty of Engineering, University of Pannonia, P.O. Box 1158, H-8210 Veszprém, Hungary
7 Division of Physical Chemistry, Rudjer Bošković Institute, Bijenička cesta 54, HR-10 000 Zagreb, Croatia
* Correspondence: asalic@fkit.hr (A.Š.); iskoric@fkit.hr (I.Š.); Tel.: +385-1-4597-101 (A.Š.); +385-1-4597-241 (I.Š.)

Abstract: A simple and efficient protocol is utilized for the transformation studies of a thiophene analog of *E*-resveratrol by photocatalytic oxygenation using an anionic and a cationic free-base porphyrin, as well as their manganese(III) complexes. The starting substrate was chosen as a representative of heterostilbenes with proven good antioxidant activity. The experiments were carried out in two photoreactor types (batch and microflow reactor) to investigate the impact of the reactor type and design on conversion and photoproduct composition. NMR spectroscopy and UHPLC/MS analyses were applied for the identification and quantification of four photoproducts (*Z*-**1**, **2**, **3**, and **4**), results of isomerization, dimerization, cyclization, and oxygenation. Different yields of photoproducts were obtained in a batch reactor and microflow reactor. In the experiments performed in a microflow reactor, *Z*-**1** was most dominant because it was constantly removed from the reaction mixture. Therefore, the formation of other products (**2**, **3**, **4**, and undefined) whose precursor is *Z*-**1** was avoided. This was not the case in the experiments performed in a batch reactor. Additionally, all the reactions tested were significantly accelerated in a microflow reactor, making it the preferred reactor type and design for the photocatalytic transformation of resveratrol derivative.

Keywords: thienostilbene; free-base porphyrins; water-soluble manganese porphyrins; photocatalytic oxygenation; microflow reactor

1. Introduction

From the early beginnings, microfluidics have positioned themselves as effective tools in many processes. Due to the specific size of the microchannel, which is usually less than 100 μm, many advantages have emerged, such as improved mass and heat transfer compared to conventional macro/batch processes, short diffusion paths, large surface-to-volume ratio, laminar flow, improved reaction selectivity, and increased reproducibility, etc. [1]. Given the above, it is believed that many processes could benefit in terms of kinetics, safety, and cost by shifting from conventional processes to microflow reactors [2]. The use of small amounts of reagents in microflow reactors also increases the safety of the process, especially when hazardous or explosive compounds are used. Regarding the use of microflow reactors in synthesis, Sambiagio and Noël [3] pointed out that microflow

technology and photochemistry are a perfect match. The authors established that in photochemistry, the reaction design should be considered along with the chemical parameters (such as the reaction conditions) and the photophysical aspect of the photocatalyst. The authors also emphasize that, unfortunately, the reactor design (batch or continuous, size, shape, material, position relative to the light source, etc.) is usually neglected by chemists. In microflow reactors, apart from the general advantages mentioned, the irradiation of the reaction mixture is improved compared to batch processes. In batch processes, the irradiation changes, depending on the distance of the light source (decreases from the flask walls towards the center of the reaction mixture), while in microflow reactors the irradiation is higher and more homogenous over the whole surface [4]. Due to the improvement of irradiation, the retention time is shortened, and higher yields of desired products can be obtained compared to batch reactors [5]. In addition, in continuous systems, products are constantly removed from the reaction mixture. This is especially important if the products obtained are also photosensitive. By removing them, the formation of byproducts is avoided, and higher yields and purities can be expected in continuously operating systems. All things considered, microflow reactors could be a good tool for the photocatalytic conversion of the resveratrol derivative.

Free-base and metalloporphyrins, possessing favorable coordination, redox, photophysical, and photochemical properties, are involved in numerous catalytic processes in both natural and artificial systems [6]. In the case of photocatalytic processes, these compounds, and their derivatives (e.g., chlorins), make the utilization of visible light possible, due to their high molar absorbances at the Soret- and Q-bands and suitable redox potentials of their ground and excited states [7]. Various porphyrins as efficient photocatalysts have been applied for the oxygenation of several types of organic compounds to generate differently functionalized derivatives [8]. Porphyrins can promote these processes in different ways, depending on their chemical composition. Metalloporphyrins with metal centers of higher oxidation numbers (already in the ground state or formed upon excitation) can either directly oxidize/oxygenize appropriate organic compounds at various sites, according to the steric and electronic conditions as well as the actual media, and/or produce reactive oxygen species (ROS) such as $HO^\bullet$ or $O_2^{\bullet-}$ radicals [9]. Characteristic representatives of such photocatalysts are manganese(III) porphyrins [8,10,11], in the case of which the following reaction steps play important role in the generation of these species in solutions [12–14].

In the first step (Equation (1)), the triplet excited-state Mn(III) complex undergoes an LMCT homolysis of the bond between the metal center and the axial ligand (e.g., HO^- in an aqueous system), producing a very reactive oxidative radical ($HO^\bullet$). In the subsequent process involving several steps, the formation of an Mn(IV) species (($P)Mn^{IV}=O$) takes place (Equation (2)).

$$(P)Mn^{III}OH + h\nu \rightarrow (P)Mn^{II} + {}^\bullet OH \tag{1}$$

$$2\,(P)Mn^{II} + O_2 \rightarrow 2\,(P)Mn^{IV}=O \tag{2}$$
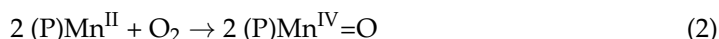
Disproportionation of the Mn(IV) complex produces an Mn(V)-oxo species of much higher reactivity (Equation (3)), hence, the latter one is most likely the major oxidative agent in these systems.

$$2\,(P)Mn^{IV}=O + H^+ \rightarrow (P)Mn^V=O + (P)Mn^{III}OH \tag{3}$$
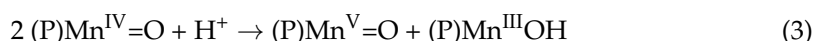
Notably, the $(P)Mn^{IV}=O$ complexes may also be involved in direct hydrogen abstraction [15].

Generation of superoxide ($O_2^{\bullet-}$) takes place via sensitization reactions with an electron transfer from the triplet excited-state Mn(III) complex to a dissolved ground-state oxygen molecule (Equation (4)) [16]. In reaction with saturated hydrocarbons, the starting (P)Mn(III) complex is regenerated, accompanied by the production of keto derivatives.

$$(P)Mn^{III} + O_2 + h\nu \rightarrow (P)Mn^{IV}\text{-}O_2^{\bullet-} \tag{4}$$

In another type of sensitization reaction, porphyrins can excite their corresponding quenchers via collisional energy transfer (ET) from their long-lived triplet state. Both free-base porphyrins and their metal complexes can be applied for this purpose. The most widely utilized example of this method is the production of singlet oxygen ($^1O_2$), which can efficiently oxidize organic pollutants in aqueous systems or kill cancer cells in photodynamic therapy [17–19]. Besides, triplet-state porphyrins may also promote the reactions of various organic compounds, especially if their activation energy is rather low. In such cases, the transferred energy, despite the considerable loss, may reach the level needed for the reaction. The photosensitized *Z-E* isomerizations are good examples of these possibilities [20,21].

In this work, transformations of the thiophene analog of *E*-resveratrol by photocatalytic oxygenation using an anionic and a cationic free-base porphyrin as well as their manganese(III) complexes, were performed in a batch and microflow reactor in order to investigate the impact of the reactor type and design on conversion, photoproduct composition, yield, and productivity.

2. Results and Discussion

In this research, as an interesting substrate for the photocatalytic reactions in batch and microflow reactor systems, resveratrol derivative *E*-**1** (Figure 1) with proven good antioxidant activity was chosen [22]. Compound *E*-**1**, with OH group at the *ortho* position and *E*-geometry of the stilbene moiety, showed to be a potent antioxidant with IC_{50} value 158.8 μmol/L. For comparison, IC_{50} value for resveratrol was found to be 77.9 μmol/L [23] and 74.0 μmol/L [24]. Compound *E*-**1** can be easily obtained, as the *E*-isomer predominates in the Wittig reaction. In our previous research [11] methyl analog of *E*-**1** (Figure 1, compound **A**) showed to be reactive in photocatalytic reactions with Mn(III) porphyrins giving photo-oxygenated products (Figure 1, structures **B** and **C**).
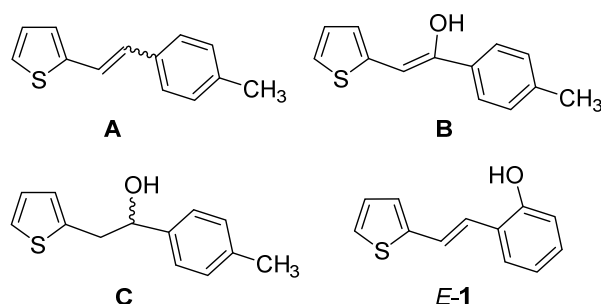
Figure 1. Structures of the substrate (**A**), its main photo-oxygenated products (**B**,**C**) [11], and of starting substrate *E*-**1**.

As a proven biologically active molecule and considering its structure as potentially suitable for photocatalytic transformations, in this paper the reactivity of compound *E*-**1** was tested using four types of porphyrins as catalysts, besides the Mn(III) also the free-base porphyrins (Figure 2, left panel). Apart from the structures of these photoactive catalysts, their UV/Vis absorption spectra are given below (Figure 2, right panel).

(a)

(b)
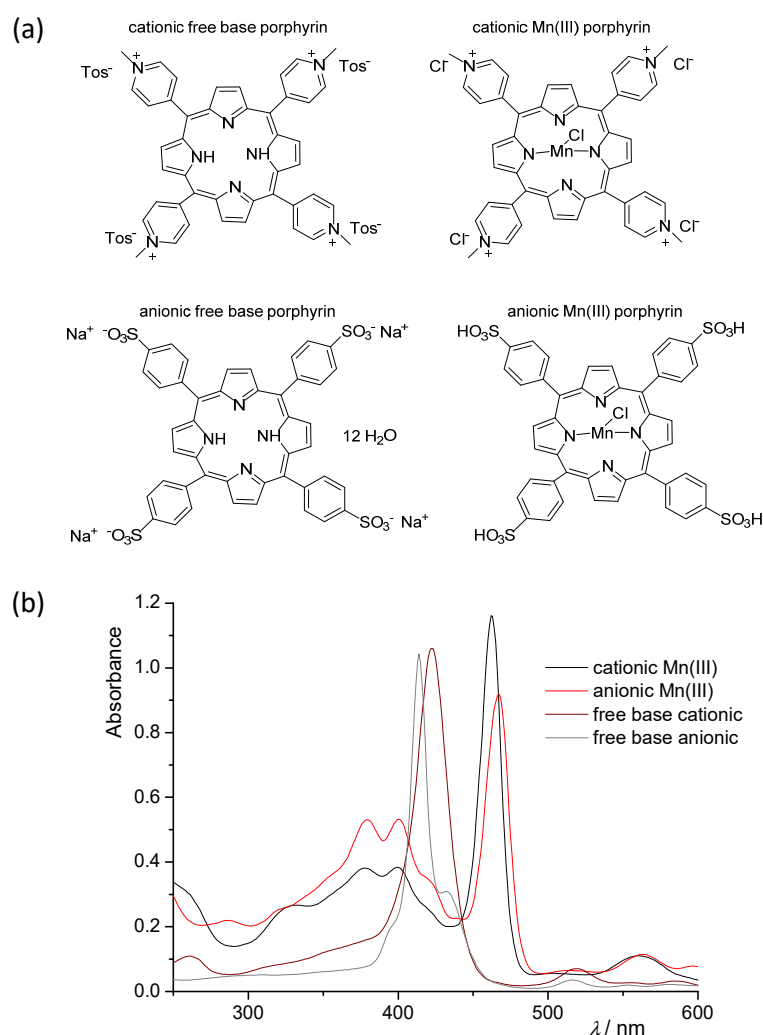
Figure 2. Structures of the used porphyrins (**a**) and their UV/Vis absorption spectra in water (**b**).

2.1. Synthesis in a Batch Reactor and Identification of Photocatalytic Transformation Products

Starting substrate, *E*-**1** was obtained in the Wittig reaction. The targeted *E*-isomer can be easily obtained [22], as the *E*-isomer predominates in the Wittig reaction mixture. According to the integrals in UHPLC analysis and ^{1}H NMR spectra, the ratio of isomers was *Z*:*E* = 1:22.5. The target product *E*-**1** was easily isolated by column chromatography. Photocatalytic reactions of *E*-**1** using four different types of porphyrins as photocatalysts (Figure 2) were performed in air-saturated acetone/water (50/50%) mixture. In order to obtain the highest conversions, the reaction time was varied from 2 to 6 h. Concentrations of porphyrins were in the range of $8.15–9.20 \times 10^{-5}$ mol dm^{-3} while the concentration of the starting *E*-**1** was 8.25×10^{-3} mol dm^{-3}.

At the end of the process of *E*-**1** catalysis with various porphyrins, different photocatalytic transformation products *Z*-**1** and **2-4** were obtained and isolated by column and thin-layer chromatography using petroleum ether/dichloromethane as eluent (Scheme 1).
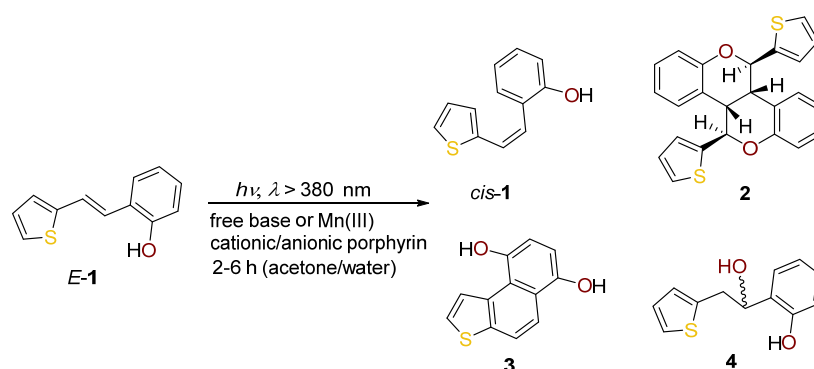
Scheme 1. Reaction pathway for the photocatalytic reactions of *E*-**1** into photoproducts *Z*-**1** and **2-4**.

According to ^{1}H NMR spectra, UPLC/MS analyses and ^{13}C NMR spectra of the reaction mixtures obtained during photocatalytic reactions under different reaction conditions, four new photoproducts were detected (Scheme 1). *E*-**1** was transformed into four characteristic photoproducts, *Z*-**1** and **2–4**. All of them were isolated by repeated column and thin-layer chromatography and characterized by spectroscopic methods. From the ^{1}H NMR spectra with recognizable patterns (Figure 3) and UPLC/MS analyses (see Section 3.3.) with characteristic masses, the structures of all the obtained photoproducts, *Z*-**1** and **2–4**, were successfully assigned. Molecular ions m/z 202 (*Z*-**1**) and m/z 216 (**3**) indicated the photoisomerization and cyclization followed by oxygenation of starting *E*-**1** (Scheme 1). It is interesting to note that an electrocyclization product such as **3** in a photocatalytic reaction with methyl-substituted analog (Figure 1, **A**) was not seen in previous research [11]. Photo-oxygenated product **4** was confirmed according to the characteristic pattern in the aliphatic part of the ^{1}H NMR spectrum and molecular ion m/z 220. It is worth mentioning that the same product **4** was isolated in 21% by oxidation of the starting *E*-**1** with *m*-CPBA [22]. NMR spectra and HRMS analyses of compounds *E*-**1**, *Z*-**1** and **2–4** are in Supplementary Materials.
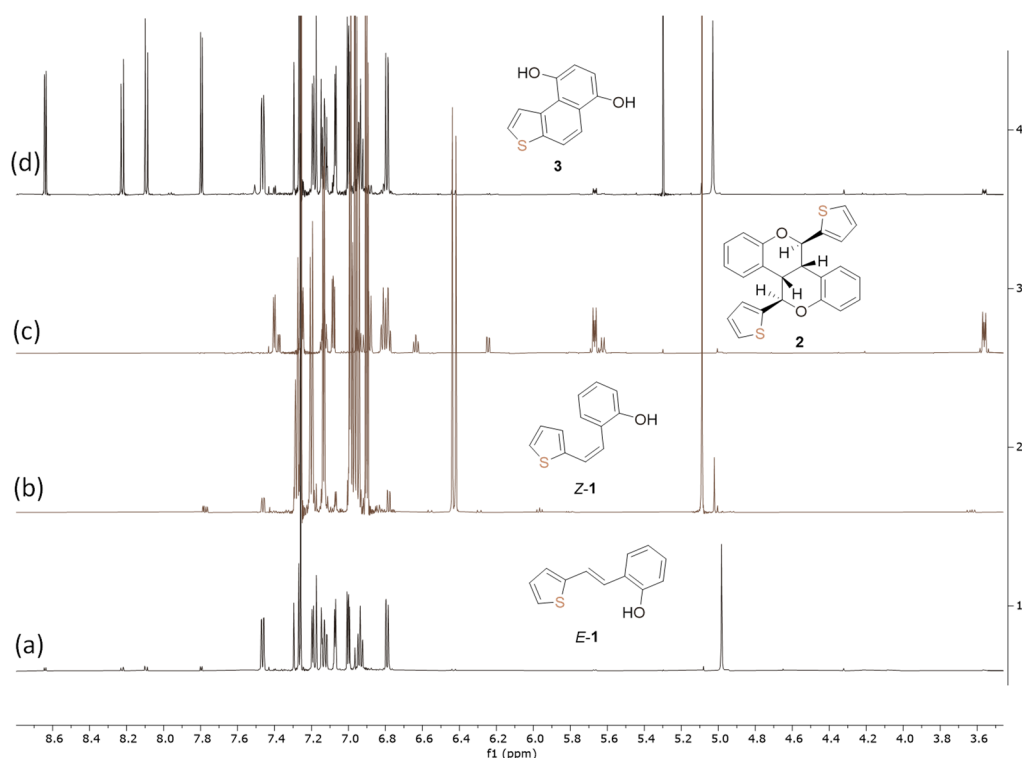
Figure 3. ^{1}H NMR spectra (CDCl$_3$) of the starting substrate *E*-**1** (**a**), and photoproducts *Z*-**1** (**b**), dimer **2** (**c**) and oxygenated cyclization product **3** (**d**).

No matter which combination of substrate and catalyst was applied, the thiophene ring remained intact in the case of all products, probably due to the appreciable aromaticity of the heteroaromatic ring. Besides, the *ortho* hydroxy aryl group was only reactive in the case of **2** and **3**, being involved in dimerization through oxygen bridges or hydroxylation at a new *ortho* position, respectively. However, these transformations did not change the strongly aromatic character of the corresponding benzene ring.

The crystal analysis unambiguously confirms the structure of the dimer **2**, obtained by the participation of two OH groups in the double cyclization into six-membered rings and with the participation of double bonds of the initial substrate *E*-**1**.

The molecular and crystal structure of the photocatalytic product **2** (Figure 4) was determined by X-ray structure analysis revealing that dimer crystallizes in space group $P2_1/n$ of the monoclinic crystal system. Its molecular symmetry is C_{2h}. The only intermolecular interactions in the crystal are C3–H3$\cdots$O2 hydrogen bonds (Figure 5; d(C–H) = 0.93 Å; d(H$\cdots$O) = 2.66 Å; d(C$\cdots$O) = 3.479(4) Å; (C–H–O) = 147°), which link two molecules, and there are only dispersion interactions between the hydrogen bonded molecules (Table 1).
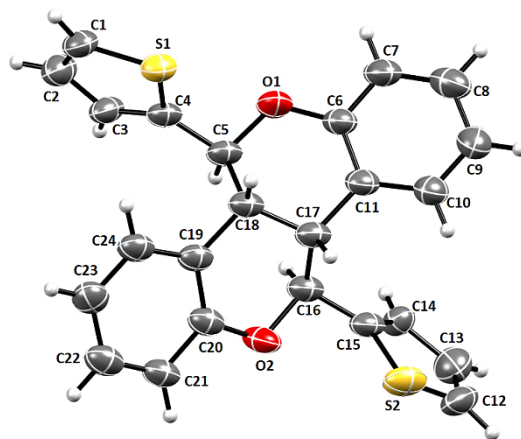
Figure 4. Molecular structure of dimeric photoproduct **2**. Displacement ellipsoids are drawn for the probability of 25% and hydrogen atoms are shown as spheres of arbitrary radii.
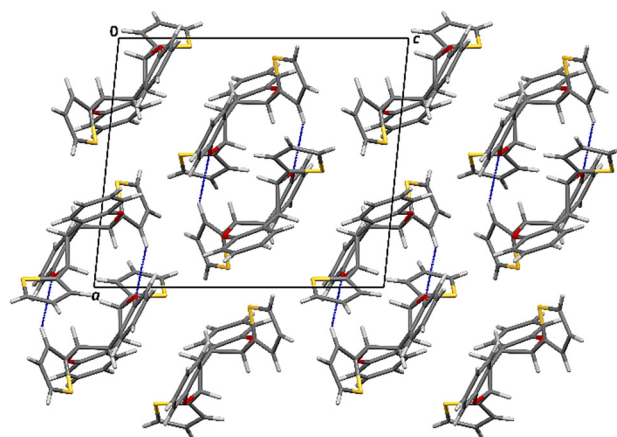
Figure 5. Crystal packing of dimer **2** viewed in the direction [010]. Two dimer molecules are linked by C3–H3$\cdots$O2 hydrogen bonds.

The isolated yields from the chromatography of the photoproducts obtained in the batch reactor using different Mn(III) and free-base cationic/anionic porphyrins are given in Table 2.

Table 1. Geometric parameters of hydrogen bonds determined from geometric analysis (A represent the hydrogen bond acceptor; Symm. Op. On A means Symmetry operation on A).

	D–H/Å	H···*A*/Å	*D*···*A*/Å	*D*–H···*A*/°	Symm. Op. on *A*
C3–H3···O2	0.93	2.66	3.479(4)	147	*x*, *y*, *z*

Table 2. Photoproducts with isolated yields (%) obtained using Mn(III) and free-base cationic/anionic porphyrins and the remained *E*-**1** for synthesis performed in a batch reactor.

Compound	Time, h	*E*-**1**	*Z*-**1**	**2**	**3**	**4**	Undefined
		%					
free-base cationic porphyrin	2	8	8	15	6	3	60
free-base anionic porphyrin	2	-	8	11	-	-	81
cationic Mn(III) porphyrin	6	6	62	-	8	2	22
anionic Mn(III) porphyrin	6	traces	25	5	4	2	64

The photoproducts unambiguously indicate that the formation of the *Z*-**1** isomer took place in the case of each porphyrin applied, independently of the charge or the presence of the metal center. This isomer is also the precursor in the production of **2** and **3**. The yields in Table 2 unequivocally suggest that the primary photoinduced reaction step of the starting compound is *E-Z* isomerization. Since *E*-**1** does not absorb in the visible range, this reaction can only take place by sensitization, in this case, through collision with a long-lived triplet excited state porphyrin. Such kind of sensitization of organic molecules by porphyrins, leading to geometric isomerization, was observed earlier, too [20,21]. The quenching of triplet-state porphyrins by *E*-**1** can efficiently compete with that of dissolved oxygen in this system. The concentration of the previous one (8.25×10^{-3} mol dm^{-3}) is at least one order of magnitude higher than the oxygen solubility in 1:1 acetone:water mixture under atmospheric pressure of air (4.1×10^{-4} mol dm^{-3} [25]). Besides, π-π (stacking) interactions between the aromatic and double-bond moieties of porphyrins and *E*-**1** can increase the quenching efficiency. Confirming this interpretation, an aromatic amine could even reductively quench triplet-state Zn(II) porphyrins (both cationic and anionic) in the aqueous system [26]. According to Table 2, anionic porphyrins (both Mn(III) and free-base) promote *E-Z* isomerization more efficiently than cationic ones do, probably because electron-richer groups ensure stronger quenching interaction. Nevertheless, singlet oxygen was also formed in the competing quenching as indicated by the oxygenated products in the systems containing free-base porphyrin (both anionic and cationic). In the presence of Mn(III) porphyrins, these products may also be formed through the interaction with manganese-oxo species, $^{\bullet}$OH, or $O_2^{\bullet-}$ radicals. However, the yields for *Z*-**1** formation are much higher than those for the other products. This suggests that the further reactions of *Z*-**1** are less favorable in the presence of Mn(III) porphyrins compared to the systems with free bases. Especially the dimer formation is much less efficient, which may be the consequence of a coordinative interaction between the monomer and the metal center. The structures of **3** and **2** indicate that monomeric ring closure and dimerization (also with ring closure, but of a different type; through an O heteroatom and forming a non-aromatic ring) are competing processes because **3** cannot be the precursor of **2**. Notably, both processes involve hydrogen abstraction, which needs oxygen. Besides, hydroxylation in the formation of **3** and **4** can only be interpreted by the reaction with singlet oxygen in the case of cationic free-base porphyrin. Metalloporphyrins may promote these processes through the production of other oxidative agents, too.

The dynamic change of conversion for free-base and Mn(III) porphyrins (anionic and cationic) obtained in a batch reactor is followed by UHPLC analysis (Figure 6).
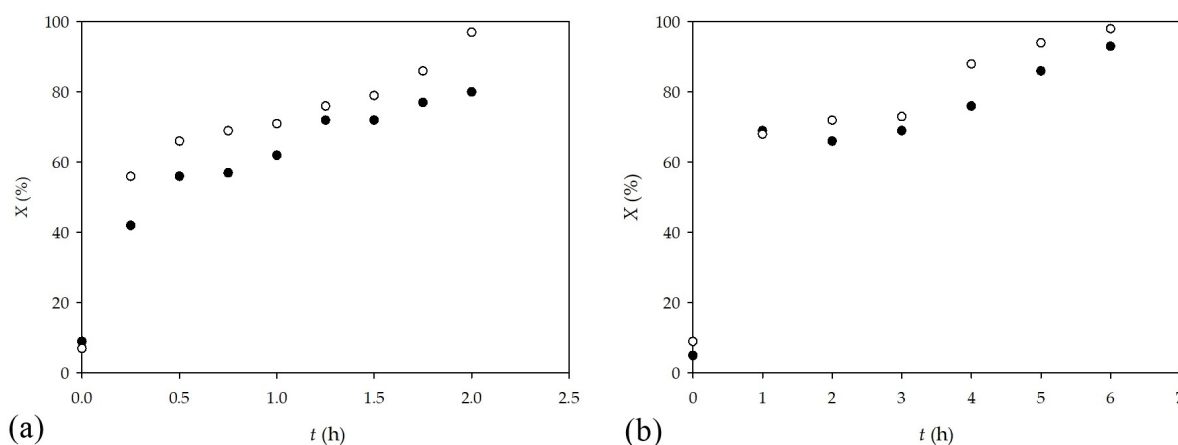
Figure 6. The dynamic change of conversion for (**a**) free-base porphyrin and (**b**) Mn(III) porphyrin (○ anionic, ● cationic) obtained by UHPLC analysis.

As can be seen, when the reaction was performed with free-base porphyrin, the reaction was faster beyond the first hour of irradiation, compared to the reaction catalyzed by Mn(III) porphyrin. Almost a complete conversion was observed after 2 h for free-base porphyrin and after 6 h for Mn(III), respectively. Interestingly, however, the dynamic change of conversion reached higher values for the reactions catalyzed by metalloporphyrins. Moreover, comparing the cationic and anionic porphyrins, the latter promoted the reaction more effectively than the former did. As already mentioned, anionic porphyrins promote *E-Z* isomerization more efficiently because the electron-richer groups ensure stronger quenching interaction. The same effect was described elsewhere [11] when the same cationic and anionic porphyrins were used as catalysts in reaction with the methyl analog of compound **1**.

2.2. Synthesis in a Microflow Reactor

As mentioned in the introduction, the reactor type and design [3] plays important role in photocatalysis. When the photocatalysis is performed in a microflow reactor the retention time is shortened and higher yields of desired products can be obtained compared to batch reactors [5]. In addition, in continuous systems such as microflow reactors, products are constantly removed from the reaction mixture. By removing them, formation of byproducts is avoided and higher yields and purities can be expected in continuously operated systems. In order to confirm these advantages, the transformations of the thiophene analogue of resveratrol *E*-**1** by photocatalytic reactions using an anionic and cationic free-base porphyrin as well as cationic and anionic Mn(III) porphyrins was shifted from batch to microflow reactor. The reactions were performed in a tubular microflow reactor (Figure 7) and the obtained results were compared with the results obtained in a batch reactor.
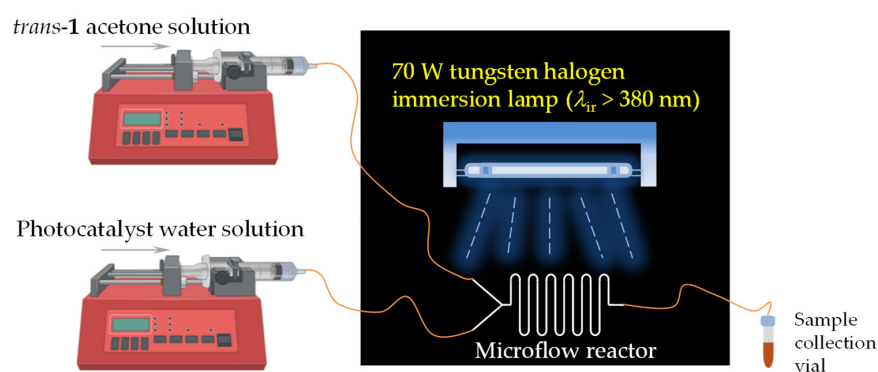
Figure 7. Experimental set-up for photocatalytic reactions performed in a microflow reactor.

The influence of the retention time on the *E*-**1** conversion using four types of porphyrins as catalysts is presented in Figure 8.

(a)

(b)
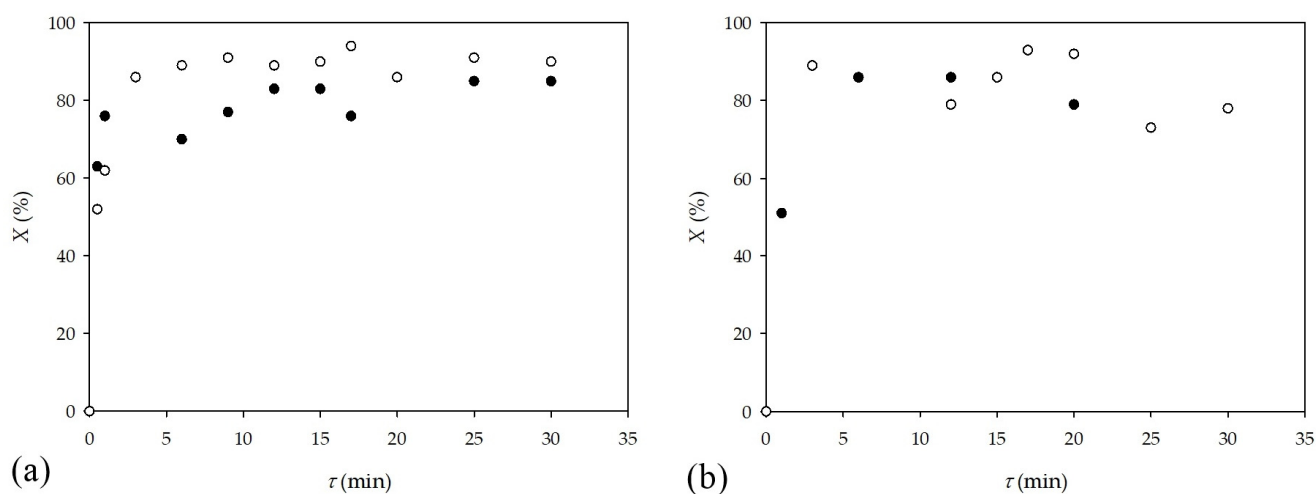
Figure 8. The influence of residence time on conversion for the reaction catalyzed by (**a**) free-base porphyrin and (**b**) Mn(III) porphyrin (○ anionic, ● cationic).

As expected, the reactions were significantly accelerated in microflow reactors, where conversions higher than 80% were observed after 5 min for free-base porphyrins and for Mn(III) porphyrins, respectively probably due to higher and more homogenous irradiation over the whole microreactor surface [4]. The same results were obtained in our previous works [11,22] where the time for complete conversion was significantly shortened in microflow reactors compared to batch reactors. As in a batch reactor, anionic porphyrins (both free-base and Mn(III)) promoted *E-Z* isomerization more efficiently than cationic ones.

Comparing the yields of photoproducts obtained in batch and microflow reactors (Table 3 and Figure 9), it can be seen that different yields of photoproducts were obtained. In a microflow reactor, *Z*-**1** was most dominant regardless of which of the four porphyrin types was used as a catalyst. As mentioned, this isomer is a product of the primary photoinduced reaction step, isomerization of *E*-**1**. In all reaction performed in a microflow reactor, the yield of *Z*-**1** was above 60%, and the yield of all other products were below 10% (Figure 9b). The difference between yield obtained in a batch and microflow reactor is more pronounced when free base porphyrin was used. As mentioned earlier, the further reactions of *Z*-**1** in the presence of metalloporphyrins are less favorable than in systems with free bases. When the free-base was used in a batch reactor (Figure 9a), the yields of products **2**, **3**, and **4** were similar to or higher than those of *Z*-**1**. *Z*-**1** is the precursor in the production of **2** and **3** and by prolonging the reaction time, more secondary products has been formed. Since in continuous microflow systems the products are constantly removed from the reaction mixture, the formation of additional products was avoided. For this reason, higher yields and purity of the *Z*-**1** product were obtained in a microflow reactor. It is also important to emphasize that the photocatalytic reaction performed in a microflow reactor is the ideal way to preoperatively obtain *Z*-**1** from the *E*-isomer since the *Z*-isomer is very difficult to obtain in the synthesis by Wittig reaction where the *E*-isomer is mainly formed.

Table 3. Yields (%) of photoproducts obtained using Mn(III) and free-base cationic/anionic por-phyrins and the remained *E*-**1** for reactions performed in a batch reactor and microflow reactor (followed by UHPLC; *t* is time and it refers to a batch reactor and τ is residence time and it is a characteristic time dimension for flow reactor).

Compound	Reactor	Time, h	*E*-1	*Z*-1	2	3	4	Unidenti-Fied	Productivity, $\mu mol\ mL^{-1}\ min^{-1}$	Ratio of Productivities
						%				
free-base cationic porphyrin	*Batch*	*t* = 2	20	31	25	2	1	21	0.0550	1/4.25
	Microflow	τ = 0.5	15	77	2	1	2	3	0.2338	
free-base anionic porphyrin	*Batch*	*t* = 2	3	15	18	-	-	64	0.0667	1/3.71
	Microflow	τ = 0.5	10	74	3	1	2	10	0.2475	
cationic Mn(III) porphyrin	*Batch*	*t* = 6	7	74	-	13	1	5	0.0213	1/10.07
	Microflow	τ = 0.5	22	66	-	6	-	6	0.2145	
anionic Mn(III) porphyrin)	*Batch*	*t* = 6	2	54	10	3	2	29	0.0225	1/9.51
	Microflow	τ = 0.5	22	62	1	1	1	13	0.2140	

(a)

(b)
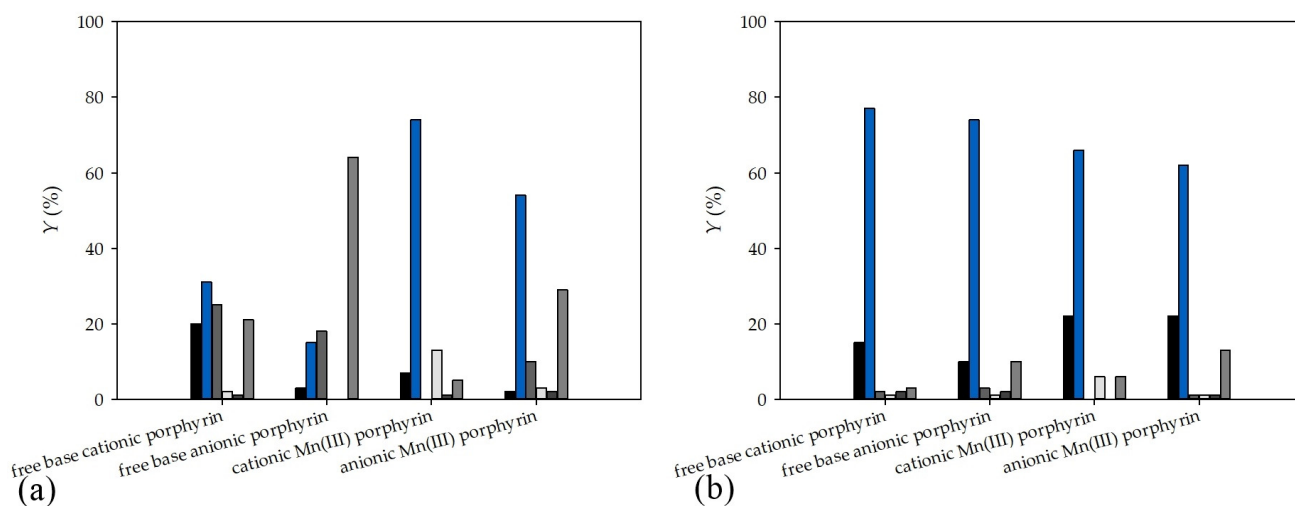
Figure 9. Yields (%) of photoproducts obtained using Mn(III) and free-base cationic/anionic por-phyrins and the remained *E*-**1** for reactions performed in (**a**) a batch reactor (2 and 6 h) and (**b**) microflow reactor (τ = 30 min) (■ *E*-1, ■ *cis*-1, ■ **2**, □ **3**, ■ **4**, ■ undefined).

Finally, the productivities for the reaction carried out in a batch reactor and a microflow reactor were calculated and compared (Table 3). As can be seen, the productivities obtained in a microflow reactor were higher than those obtained in a batch reactor. Comparing the ratio of productivities (batch vs. microflow reactor) of free-base and Mn(III) porphyrin, the higher ratio was obtained using Mn(III) porphyrin. Although the yields were slightly lower for the reactions carried out with the Mn(III) porphyrin, the reaction was significantly accelerated for this catalyst in a microflow reactor compared to the free-base porphyrin considering that the maximum yield was obtained for 6 h in a batch reactor and for 5 min residence time in a microflow reactor. When a free-base porphyrin was used, the reaction in a microflow reactor was also significantly accelerated, but the time difference was slightly smaller (2 h for the batch reactor and 5 min for the microflow reactor).

Combining all the results, and comparing the reaction/residence times, conversions, yields, and productivities for reactions performed in a batch reactor and microflow reactor, it can be seen that the microflow reactor is the preferred type of reactor for photocatalytic oxygenation of the resveratrol derivative.

3. Materials and Methods

3.1. General

All used solvents were commercially available and were purified by distillation (Gram Mol, Zagreb, Croatia). The following porphyrins were used in the experiments: (1) cationic free-base porphyrin, 5,10,15,20-tetrakis(1-methylpyridinium-4-yl)porphyrin (tetra tosylate salt) (H_2TMPyP^{4+} (+ 4 $CH_3C_6H_4SO_3^-$, TMP-1363, Frontier Scientific, Newark, NJ, USA); (2) cationic Mn(III)porphyrin, Mn(III) 5,10,15,20-tetrakis (1-methylpyridinium-4-yl)porphyrin pentachloride (T40809, Frontier Scientific, Newark, NJ, USA); (3) anionic free-base porphyrin: 5,10,15,20-tetrakis(4-sulfonatophenyl)porphyrin (tetrasodium salt dodecahydrate) (T40699, Frontier Scientific, Newark, NJ, USA, H_2TSPP^{4-} (+4 Na^+ counterions); (4) anionic Mn(III) porphyrin: Mn(III) 5,10,15,20-tetrakis (4-sulfonatophenyl)porphyrin chloride (acid form) (Mn1239, Frontier Scientific, Newark, NJ, USA). Anhydrous magnesium sulfate, $MgSO_4$ was used for drying organic layers after extractions (Sigma-Aldrich, St. Louis, MO, USA). The products were purified by column and thin-layer chromatography on silica gel (Fluka 60 Å, technical 20 × 20 cm, Fluka Chemie GmbH, Buchs, Switzerland). The ^{1}H and ^{13}C-NMR spectra were recorded on a Bruker Avance spectrometer (Coventry, UK) at 600 MHz with $CDCl_3$ as a solvent and tetramethylsilane as a reference. The reactions giving the photoproducts Z-**1** and **2**–**4** was followed by UHPLC and confirmed with an MS detector equipped with an ESI source (Agilent Technologies, Santa Clara, CA, USA). UV spectra were recorded on UV/Vis spectrophotometer (Varian Cary 50 UV/Vis, Lexington, MA, USA). Photocatalytic transformation reactions were performed in a thermostated cylindrical home-made batch photoreactor (50 cm^3) and microflow photoreactors (5.2 mm^3) (Micronit BV, Enschede, Netherlands). The starting heterocyclic aldehyde used was a purchased chemical (Sigma-Aldrich, St. Louis, MO, USA).

3.2. Typical Experimental Procedure for the Synthesis of E-**1**

Wittig reaction provided the mixture of *E*- and *Z*-isomers of compound **1** [22]. In a three-necked flask, purged with nitrogen, phosphonium salt (1 eq, 9.44 mmol) was added to absolute ethanol (100 mL, 3 Å sieves). Thiophene-2-carbaldehyde (1 eq, 9.44 mmol), was then added and sodium ethoxide (1.1 eq) was added finally dropwise to the reaction solution. The reaction mixture was stirred for 72 h, ethanol was then removed under reduced pressure. The raw product was extracted with toluene p.a. and dried over anhydrous $MgSO_4$. According to the integrals in UHPLC analysis and ^{1}H NMR spectra, the ratio of the isomers of **1** was Z:E = 1:22.5. The target product E-**1** was isolated in the last fractions by column chromatography.
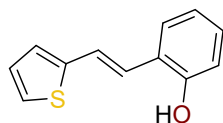
E-**1**

(E)-2-(2-(thiophen-2-yl)vinyl)phenol (*E*-**1**) [22]: 495 mg (isolated 82%), white powder; m.p. = 126–127 °C; R_f (PE/DCM = 50%) = 0.33; UV (CH_3CN) λ_{max}/nm (ε/dm^{3}mol^{-1}cm^{-1}) 335 (25412); ^{1}H-NMR ($CDCl_3$, 600 MHz) δ/ppm: 7.46 (dd, *J* = 7.7, 1.6 Hz, 1H), 7.28 (dt, *J* = 16.1, 0.8 Hz, 1H), 7.20–7.16 (m, 2H), 7.15–7.10 (m, 1H), 7.07 (dt, *J* = 3.7, 0.9 Hz, 1H), 6.99 (dd, *J* = 5.1, 3.5 Hz, 1H), 6.93 (td, *J* = 7.5, 1.2 Hz, 1H), 6.78 (dd, *J* = 8.1, 1.2 Hz, 1H), 4.97 (s, 1H); ^{13}C-NMR ($CDCl_3$, 150 MHz) δ/ppm: 152.5 (s), 142.0 (s), 126.9 (d), 125.9 (d), 125.1(d), 124.1 (d), 122.4 (d), 122.4 (s), 121.8 (d), 120.4 (d), 118.7 (d), 114.3 (d); MS (ESI) *m/z* (%, fragment): 203 (100).

3.3. Typical Experimental Procedure for the Photocatalytic Reactions in a Batch Reactor

There were four experimental routes of photocatalytic reactions using free-base cationic or anionic and cationic or anionic Mn(III) complexes. Synthesized E-**1** and the free-base cationic/anionic or cationic/anionic Mn(III) porphyrins were dissolved in a solution of

50 cm^3 mixture of acetone/water (1:1) at pH 7. The solutions were irradiated with a 70 W tungsten halogen immersion lamp (Philips, $\lambda_{ir} > 380$ nm) in a thermostated 50 cm^3 cylindrical photoreactor. During 2 h (free-base cationic/anionic) and 6 h (cationic/anionic Mn(III) porphyrins), a stream of air was passed through the solution. Concentrations of porphyrins were as follows: free-base cationic 8.50×10^{-5} mol dm^{-3} and anionic 8.07×10^{-5} mol dm^{-3}; Mn(III) cationic 9.20×10^{-5} mol dm^{-3} and Mn(III) anionic 8.15×10^{-5} mol dm^{-3}. The concentration of the starting *E*-**1** was 8.25×10^{-3} mol dm^{-3}. After irradiation, acetone was evaporated from the reaction mixture. The rest of the solution was extracted with diethyl ether and dried over MgSO$_4$. Solid residues remained after evaporating the solvent under reduced pressure. In each experiment, the products were isolated by column chromatography and TLC using petroleum ether/dichloromethane as an eluent. In the first fractions, the dimeric product **2** was isolated which was slightly faster on the column than the *Z*-**1**, followed by the *E*-**1** and product **3** with equal *Rf* values, and finally in the last fractions product, **4** was obtained as the slowest one. The isolated yields of the photoproduct *Z*-**1** and **2-4** as well as the quantities of the remained *E*-**1** are given in Table 2 in the Section 2.
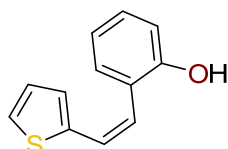
Z-**1**

(Z)-2-(2-(thiophen-2-yl)vinyl)phenol (*Z*-**1**): 60 mg (isolated max. 62%), colorless oil; R_f (PE/DCM = 50%) = 0.44; UV (CH$_3$CN) λ_{max}/nm (ε/dm^{3}mol^{-1}cm^{-1}) 289 (26313); ^{1}H-NMR (CDCl$_3$, 600 MHz) δ/ppm: 7.28 (tdd, *J* = 7.9, 1.7, 0.7 Hz, 1H), 7.20 (dt, *J* = 7.7, 1.2 Hz, 1H), 7.13 (dt, *J* = 5.1, 0.9 Hz, 1H), 7.01–6.93 (m, 4H), 6.90 (dd, *J* = 5.1, 3.6 Hz, 1H), 6.43 (d, *J* = 11.6 Hz, 1H), 5.08 (s, 1H); ^{13}C-NMR (CDCl$_3$, 150 MHz) δ/ppm: 153.2 (s), 138.7 (s), 129.2 (d), 128.3 (d), 127.6 (d), 126.7 (s), 125.4 (d), 125.1 (d), 123.5 (d), 122.9 (d), 118.9 (d), 114.4 (d); MS (ESI) *m/z* (%, fragment): 203 (100).
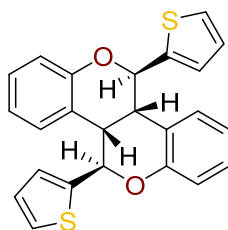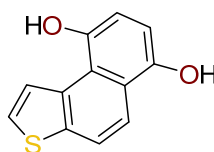
2　　　　　　　　　　**3**

(4bS,5R,10bS,11R)-5,11-di(thiophen-2-yl)-4b,5,10b,11-tetrahydrochromeno[4,3-c]chromene (**2**): 6 mg (isolated max. 15%); white powder; m.p. = 155–158 °C; R_f (PE/DCM = 50%) = 0.65; UV (CH$_3$CN) λ_{max}/nm (ε/dm^{3}mol^{-1}cm^{-1}) 283 (25196), 276 (27036); ^{1}H-NMR (CDCl$_3$, 600 MHz) δ/ppm: 7.40 (dd, *J* = 5.1, 1.2 Hz, 1H), 7.25 (dd, *J* = 4.4, 1.5, Hz, 1H), 7.13 (dd, *J* = 8.7, 1.8 Hz, 1H), 7.09–7.07 (m, 1H), 6.88 (dd, *J* = 8.1, 1.2 Hz, 1H), 6.83–6.76 (m, 2H), 5.70–5.64 (m, 1H), 3.60–3.53 (m, 1H); ^{13}C-NMR (CDCl$_3$, 150 MHz) δ/ppm: 144.3 (s), 130.8 (s), 128.1 (d), 127.1 (d), 127.0 (d), 126.6 (d), 125.7 (d), 125.4 (s), 121.5 (d), 117.9 (d), 42.6 (d), 29.7 (d); MS (ESI) *m/z* (%, fragment): 342 (5), 301 (15), 279 (100).

Naphtho[2,1-b]thiophene-6,9-diol (**3**): 3 mg (isolated max. 8%); yellow oil; R_f (PE/DCM = 50%) = 0.33; UV (CH$_3$CN) λ_{max}/nm (ε/dm^{3}mol^{-1}cm^{-1}) 290 (16512); ^{1}H-NMR (CDCl$_3$, 600 MHz) δ/ppm: 8.64 (dd, *J* = 5.6, 0.9 Hz, 1H), 8.22 (dd, *J* = 8.4, 0.9 Hz, 1H), 8.09 (d, *J* = 8.3 Hz, 1H), 7.80 (d, *J* = 5.6 Hz, 1H), 6.96 (s, 2H); MS (ESI) *m/z* (%, fragment): 216 (100).

3.4. Experimental Procedure for Photocatalytic Reactions in Microflow Reactors

The selected glass microflow reactor (Micronit BV, Enschede, Netherlands) was equipped with Y-shaped inlets and one outlet with the following dimensions

width $\times$ depth $\times$ length = 250 μm $\times$ 50 μm $\times$ 332 cm and volume of 4.15 μL. The substrate and catalysts concentrations were the same as in a batch experiment (*E*-**1** 8.25 $\times$ 10^{-3} mol dm^{-3}, free-base cationic catalyst 8.50 $\times$ 10^{-5} mol dm^{-3}, free-base anionic catalyst 8.07 $\times$ 10^{-5} mol dm^{-3}, Mn(III) cationic catalyst 9.20 $\times$ 10^{-5} mol dm^{-3}, and Mn(III) anionic catalyst 8.15 $\times$ 10^{-5} mol dm^{-3} and). Two syringe pumps (PHD 4400 Syringe Pump Series, Harvard Apparatus, Holliston, MA, USA) equipped with high-pressure stainless-steel syringes (8 mL, Harvard Apparatus, New York City, NY, USA) were used to supply substrate and catalyst in a microflow reactor. One syringe pump was used to supply the selected catalyst and another to supply the substrate. The flow ratio of both streams was set to be 1:1 in all experiments to ensure the same conditions as in the batch reactor. Flow rates investigated in this research were in the range of q = 0.138–8.3 μL/min which corresponded to residence times of τ = 0.5–30 min. The microflow reactor was placed under the UV lamp at a distance from the lamp of 2 mm. In all experiments, outflows (approximately 100 μL) were collected in vials, and samples were analyzed.

3.5. X-ray Crystallography

Single crystals were measured on an XtaLAB Synergy diffractometer (Rigaku OD, Tokyo, Japan), at room temperature [293(2) K], with micro-focus sealed X-ray tube CuKα (1.54184 Å) radiation. Data reduction and numerical absorption correction were done with The CrysAlisPRO package (Rigaku OD, Tokyo, Japan, 2018).

SHELXS97 [27] was used for structure solution and SHELXL2018 [28] for the refinement. The model was refined using the full matrix least-squares refinement. Non-hydrogen atoms were refined anisotropically. Hydrogen atoms were located in a different Fourier map and refined as a mixture of free and riding entities. PLATON [29] was used for molecular geometry calculations, and ORTEP-3 [30] and CCDC-Mercury [31] were used for molecular graphics. Crystallographic and structure refinement data are shown in Table 4.

Table 4. Crystallographic data and structure refinement details for dimer **2**.

Compound	2
Empirical formula	$C_{24}H_{18}O_2S_{1.8}$
Formula wt./g mol^{-1}	393.96
Crystal dimensions/mm	$0.3 \times 0.25 \times 0.1$
Space group	$P2_1/n$
a/Å	12.3164(7)
b/Å	11.2022(11)
c/Å	14.2889(9)
α/°	90
β/°	95.702(5)
γ/°	90
Z	4
V/Å^3	1961.7(3)
D_{calc}/g cm^{-3}	1.334
μ/mm^{-1}	2.355
Θ range/°	4.523–80.415
T(K)	293(2)
Radiation wavelength	1.54184 (CuK$_\alpha$)
Diffractometer type	XtaLAB Synergy, Dualflex, HyPix
Range of h, k, l	$-15 > h > 15;$ $-13 > k > 14;$ $-18 > l > 16$
Reflections collected	15177
Independent reflections	4003
Observed reflections ($I \geq 2\sigma$)	1866
R_{int}	0.1331
R (F)	0.0951
R_w (F^2)	0.3112
No. of parameters, restraints	255, 0
Goodness of fit	0.952
$\Delta\rho_{max}, \Delta\rho_{min}$ (eÅ^{-3})	0.443; −0.289

Supplementary crystallographic data for this paper can be obtained free of charge via www.ccdc.cam.ac.uk/conts/retrieving.html (or from the Cambridge Crystallographic Data Centre, 12, Union Road, Cambridge CB2 1EZ, UK; fax: +44 1223 336033; or deposit@ccdc.cam.ac.uk). CCDC-2212442 contains supplementary crystallographic data for this paper.

4. Conclusions

Nowadays, flow chemistry is already well known and developed field. Many times, as is the case with this work, it has been proven that the use of microflow reactors can better control the formation of the desired products than is possible in batch reactors. It is possible to obtain cleaner products, and achieve high conversions and high productivity, all in a significantly shorter time than is possible in a batch reactor.

The starting substrate thiophene analog of *E*-resveratrol was chosen as a representative of heterostilbenes with proven good antioxidant activity for the transformations studies of photocatalytic oxygenation using an anionic and a cationic free-base porphyrin as well as their Mn(III) complexes. The experiments were carried out in two photoreactor types (batch and microflow reactor) to investigate the impact of reactor type and design on conversion and product composition. From the preparative synthesis in a batch reactor, the four photoproducts (*Z*-**1**, **2**, **3**, and **4**), were isolated and the NMR spectroscopy, UHPLC/MS, and crystal structure analyses were applied for the identification and quantification of *Z*-**1**, **2**, **3** and **4**, as results of isomerization, dimerization, cyclization, and oxygenation, respectively. To produce photoproduct *Z*-**1**, a microflow reactor was the performable reactor type. The desired product was obtained in a much shorter time, with a higher yield than for the reaction performed in a batch reactor. Since the product was constantly removed from the reaction mixture, the formation of unwanted products was minimized.

As a future scope, in the research of heterostilbenes photochemistry, it is planned to examine the comparison of direct illumination of the substrates at lower wavelengths with photocatalytic reactions of the molecules, and to rationalize experimentally and computationally the nature and ratio of the obtained products, as well as to analyze the influence of the reactor design and type. As it is expected that more model compounds should be used to confirm the advantages of microflow reactor in the photocatalytic transformations of heterostilbene photochemistry, this will be also the scope of our following investigations.

References

1. Noël, T.; Naber, J.R.; Hartman, R.L.; Mcmullen, J.P.; Jensen, K.F.; Buchwald, S.L. Palladium-catalyzed amination reactions in flow: Overcoming the challenges of clogging via acoustic irradiation. *Chem. Sci.* **2011**, *2*, 287–290. [CrossRef]
2. Rashmi Pradhan, S.; Colmenares-Quintero, R.F.; Colmenares Quintero, J.C. Designing Microflowreactors for photocatalysis using sonochemistry: A systematic review article. *Molecules* **2019**, *24*, 3315. [CrossRef]
3. Sambiagio, C.; Noël, T. Flow photochemistry: Shine some light on those tubes! *Trends Chem.* **2019**, *2*, 92–106. [CrossRef]
4. Oelgemoeller, M. Highlights of photochemical reactions in microflow reactors. *Chem. Eng. Technol.* **2012**, *35*, 1144–1152. [CrossRef]
5. Chandrasekhar, D.; Borra, S.; Kapure, J.S.; Shivaji, G.S.; Srinivasulu, G.; Maurya, R.A. Visible-light photoredox catalysis: Direct synthesis of fused-carbolines through an oxidation/[3 + 2]cycloaddition/oxidative aromatization reaction cascade in batch and flow microreactors. *Org. Chem. Front.* **2015**, *2*, 1308–1312. [CrossRef]
6. Barona-Castaño, J.C.; Carmona-Vargas, C.C.; Brocksom, T.J.; Oliveira, K.T. Porphyrins as catalysts in scalable organic reactions. *Molecules* **2016**, *21*, 310. [CrossRef]
7. Silva, R.C.; Silva, L.O.; Andrade Bartolomeu, A.; Brocksom, T.J.; Oliveira, K.T. Recent applications of porphyrins as photocatalysts in organic synthesis: Batch and continuous flow approaches. *Beilstein J. Org. Chem.* **2020**, *16*, 917–955. [CrossRef] [PubMed]
8. Šagud, I.; Škorić, I. Photocatalytic oxygenation by water-soluble metalloporphyrins as a pathway to functionalized polycycles. *Int. J. Photoenergy* **2018**, *2018*, 1017957. [CrossRef]
9. Hong, Y.H.; Han, J.W.; Jung, J.; Nakagawa, T.; Lee, Y.M.; Nam, W.; Fukuzumi, S. Photocatalytic oxygenation reactions with a cobalt porphyrin complex using water as an oxygen source and dioxygen as an oxidant. *J. Am. Chem. Soc.* **2019**, *141*, 9155–9159. [CrossRef]
10. Vuk, D.; Horváth, O.; Škorić, I. New functionalized polycycles obtained by photocatalytic oxygenation using Mn(III) porphyrins in basic media. *Catalysts* **2019**, *9*, 304. [CrossRef]
11. Mlakić, M.; Šalić, A.; Bačić, M.; Zelić, B.; Šagud, I.; Horváth, O.; Škorić, I. Photocatalytic oxygenation of heterostilbenes—Batch versus microflow reactor. *Catalysts* **2021**, *11*, 395. [CrossRef]
12. Zhang, R.; Horner, J.H.; Newcomb, M. Laser flash photolysis generation and kinetic studies of porphyrin−manganese−oxo intermediates. Rate constants for oxidations effected by porphyrin−Mn(V)−oxo species and apparent disproportionation equilibrium constants for porphyrin−Mn(IV)−oxo species. *J. Am. Chem. Soc.* **2005**, *127*, 6573–6582. [CrossRef]
13. Newcomb, M.; Zhang, R.; Pan, Z.; Harischandra, D.; Chandrasena, R.; Horner, J.; Martinez, E., II. Laser flash photolysis production of metal-oxo derivatives and direct kinetic studies of their oxidation reactions. *Catal. Today* **2006**, *117*, 98–104. [CrossRef]
14. Zhang, R.; Newcomb, M. Laser Flash Photolysis generation of high-valent transition metal−oxo species: Insights from kinetic studies in real time. *Acc. Chem. Res.* **2008**, *41*, 468–477. [CrossRef] [PubMed]
15. Baglia, R.A.; Zaragoza, J.P.T.; Goldberg, D.P. Biomimetic reactivity of oxygen-derived manganese and iron porphyrinoid complexes. *Chem. Rev.* **2017**, *117*, 13320–13352. [CrossRef] [PubMed]
16. Jung, J.; Ohkubo, K.; Goldberg, D.P.; Fukuzumi, S. Photocatalytic oxygenation of 10-methyl-9,10-dihydroacridine by O_2 with manganese porphyrins. *J. Phys. Chem. A* **2014**, *118*, 6223–6229. [CrossRef] [PubMed]
17. Quina, F.H.; Medeiros Silva, G.T. The photophysics of photosensitization: A brief overview. *J. Photochem. Photobiol.* **2021**, *7*, 100042. [CrossRef]
18. Buglak, A.A.; Filatov, M.A.; Hussain, M.A.; Sugimoto, M. Singlet oxygen generation by porphyrins and metalloporphyrins revisited: A quantitative structure-property relationship (QSPR) study. *J. Photochem. Photobiol. A* **2020**, *403*, 112833. [CrossRef]
19. Kou, J.; Dou, D.; Yang, L. Porphyrin photosensitizers in photodynamic therapy and its applications. *Oncotarget* **2017**, *8*, 81591–81603. [CrossRef]
20. Prashanthi, S.; Kumar, P.H.; Siva, D.; Lanke, S.R.; Rao, V.J.; Basak, S.; Bangal, P.R. Photochemical *E*(*trans*)–*Z*(*Z*)–*E* isomerization of an amphiphilic cholest-5-en-3β-yl(*E*)-9-anthraceneprop-2-enoate on solid substrate. *J. Phys. Chem. C* **2011**, *115*, 20682–20688. [CrossRef]
21. Isokuortti, J.; Kuntze, K.; Virkki, M.; Ahmed, Z.; Vuorimaa-Laukkanen, E.; Filatov, M.A.; Turshatov, A.; Laaksonen, T.; Priimagi, A.; Durandin, N.A. Expanding excitation wavelengths for azobenzene photoswitching into the near-infrared range via endothermic triplet energy transfer. *Chem. Sci.* **2021**, *12*, 7504–7509. [CrossRef]
22. Mlakić, M.; Rajič, L.; Ljubić, A.; Vušak, V.; Zelić, B.; Gojun, M.; Odak, I.; Čule, I.; Šagud, I.; Šalić, A.; et al. Synthesis of new heterocyclic resveratrol analogues in milli- and microreactors: Intensification of the Wittig reaction. *J. Flow Chem.* **2022**. [CrossRef]
23. Gülçin, I. Antioxidant properties of resveratrol: A structure–activity insight. *Innov. Food Sci. Emerg. Technol.* **2010**, *11*, 210–218. [CrossRef]
24. Fauconneau, B.; Waffo-Teguo, P.; Huguet, F.; Barrier, L.; Decendit, A.; Merillon, J.M. Comparative study of radical scavenger and antioxidant properties of phenolic compounds from vitis vinifera cell cultures using in vitro tests. *Life Sci.* **1997**, *61*, 2103–2110. [CrossRef]
25. Tsuji, K.; Ichikawa, K.; Yamatoto, H.; Tokunaga, J. Solubilities of oxygen and nitrogen in acetone-water mixed solvent. *Kagaku Kogaku Ronbunshu* **1987**, *13*, 825–830. [CrossRef]
26. Schmitt, M.; Erikson, P.R.; McNeill, K. Triplet-state dissolved organic matter quantum yields and lifetimes from direct observation of aromatic amine oxidation. *Environ. Sci. Technol.* **2017**, *51*, 13151–13160. [CrossRef]
27. Farrugia, L.J. WinGX suite for small-molecule single-crystal crystallography. *J. Appl. Cryst.* **1999**, *32*, 837–838. [CrossRef]
28. Sheldrick, G.M. A short history of SHELX. *Acta Crystallogr. A* **2008**, *64*, 112–122. [CrossRef]

29. Spek, A.L. Structure validation in chemical crystallography. *Acta Crystallogr. D* **2009**, *D65*, 148–155. [CrossRef]
30. Farrugia, L.J. It ORTEP-3 for Windows—A Version of It ORTEP-III with a Graphical User Interface (GUI). *J. Appl. Cryst.* **1997**, *30*, 565. [CrossRef]
31. Macrae, C.F.; Edgington, P.R.; McCabe, P.; Pidcock, E.; Shields, G.; Taylor, R.; Towler, M.; van de Streek, J. Mercury: Visualization and analysis of crystal structures. *J. Appl. Cryst.* **2006**, *39*, 453–457. [CrossRef]